HEALTH AND MEDICINE

Targeted pathological collagen delivery of sustained-release rapamycin to prevent heterotopic ossification

Yangwu Chen[1,2,3,4]*, Weiliang Shen[1,2,3,4]*, Chenqi Tang[1,2,3,4], Jiayun Huang[1,2,3,4], Chunmei Fan[1,2,3,4], Zi Yin[1,2,3,4], Yejun Hu[1,2,3,4], Weishan Chen[1,2,3,4], Hongwei Ouyang[1,2,3,4], Yiting Zhou[1,5†], Zhengwei Mao[6†], Xiao Chen[1,2,3,4†]

Heterotopic ossification (HO) in connective tissues like tendons and ligaments severely damages tissue structure. The pathogenesis of HO remains unclear but may involve mTOR. The results presented here indicate that tendon stem/progenitor cells do not undergo osteochondrogenic differentiation when mTOR signaling is inactivated by gene knockout or rapamycin (RAPA) treatment. Meanwhile, it is necessary to deliver RAPA to the injured sites and avoid disturbing the normal tendon. A RAPA delivery system, developed using collagen hybrid peptide (CHP) to modify the surface of poly(lactic-*co*-glycolic acid) (PLGA) nanoparticles, targeted RAPA specifically to pathological tendon collagen. The CHP-PLGA-RAPA nanoparticles showed excellent pathological collagen affinity, sustained-release ability, and bioactivity. In a mouse model of tendon HO, CHP-PLGA-RAPA nanoparticles specifically bound to pathological tendon and strongly suppressed HO progression. The mTOR signaling pathway appears to be a viable therapeutic target for tendon HO, and CHP-PLGA nanoparticles may be valuable for the treatment of tendon-related diseases.

INTRODUCTION

Approximately 30% of clinical consultations for musculoskeletal system diseases involve tendon injury (*1*). The tendon lacks cells and blood vessels, so its ability for endogenous repair is inadequate. For this reason, most cases of tendon injury progress to tendinopathy. The clinical symptoms of chronic tendinopathy mainly manifest as pain, swelling, and inability to perform normal activities (*2*–*4*). One subtype of tendinopathy is tendon heterotopic ossification (HO), which damages the structure of the tendon tissue itself, aggravates symptoms, and severely impairs tendon function (*5*).

Endochondral ossification can include the development of ectopic calcification in connective tissues, including tendons (*6*, *7*). A previous study has demonstrated that injured tendons in humans express higher levels of cartilage-associated matrix proteins and marker genes (*8*). In addition, tendon stem/progenitor cells (TSPCs), when localized in the inflammatory niche of tendinopathy, exhibit a strong tendency to differentiate into chondroid and osteoid tissues (*9*). Consequently, we hypothesized that early therapeutic intervention in tendon injury could prevent the onset of inappropriate TSPC differentiation, thereby protecting tendons from ectopic ossification. Currently, the main challenges are the lack of knowledge regarding the critical ossification mechanisms and the absence of an appropriate system to deliver drugs precisely to the pathological tendon.

Ectopic osteogenesis in a variety of tissues may be under the control of the mammalian target of rapamycin (RAPA) (mTOR) signaling pathway, a crucial regulator of cell biological processes, including cell growth, metabolism, and protein synthesis (*10*–*13*). Several studies have implicated mTOR in tendon and ligament ossification, although different perspectives have prevented a consensus on underlying mechanisms. For example, Jiang *et al.* (*14*) reported that mTOR inhibition can decelerate rat tendon ossification after Achilles tenotomy. By contrast, another transcriptome-level investigation demonstrated down-regulation of mRNA expression of the mTOR signaling pathway in human ossified ligament (*15*), but up-regulation of circular RNA expression (*15*). For these reasons, further exploration of mTOR function in tendon HO is essential.

In the present study, tendon tissue–specific mTOR gene knockout mice were used to demonstrate the essential function of mTOR signaling in the progression of tendon HO. We hypothesized that the inhibitor RAPA could prevent tendon HO by modulating the abnormal differentiation of TSPCs. However, we recently found that mTOR also mediates the normal tenogenic differentiation of TSPCs (*16*). Accordingly, direct injection of RAPA might be unsuitable for treating tendinopathy because tendon injury or tendon ossification usually occurs in a local position and not along the whole tendon.

We have fabricated a drug delivery system that can target and bind to injured collagen. When a lesion appears on a tendon, inflammatory factors initiate the expression of matrix metalloproteinase, with a resulting degradation of the extracellular matrix and damage to the inherent triple helix structure of collagen (*1*, *17*). Collagen hybrid peptide (CHP) is a synthetic molecule that specifically binds to this intact and denatured collagen structure (*18*–*20*). We devised a drug delivery system consisting of nanoparticles made from poly(lactic-*co*-glycolic acid) (PLGA), a biocompatible and biodegradable material, with surfaces covered with CHP. This system facilitated the accurate positioning and integration of PLGA onto a pathological tendon while avoiding healthy tendons. CHP-PLGA nanoparticles containing encapsulated RAPA were able to provide a sustained release of RAPA to treat the pathological tendon of a mouse model of HO.

[1]Dr. Li Dak Sum–Yip Yio Chin Center for Stem Cells and Regenerative Medicine and Department of Orthopedic Surgery of The Second Affiliated Hospital, Zhejiang University School of Medicine, Hangzhou, China. [2]Key Laboratory of Tissue Engineering and Regenerative Medicine of Zhejiang Province, Zhejiang University School of Medicine, Hangzhou, China. [3]Department of Sports Medicine, Zhejiang University School of Medicine, Hangzhou, China. [4]China Orthopedic Regenerative Medicine Group (CORMed), Hangzhou, China [5]Department of Biochemistry and Molecular Biology, School of Medicine, Zhejiang University, 866 Yu Hang Tang Road, Hangzhou, Zhejiang 310058, China. [6]MOE Key Laboratory of Macromolecular Synthesis and Functionalization, Department of Polymer Science and Engineering, Zhejiang University, Hangzhou 310027, China.
*These authors contributed equally to this work.
†Corresponding author. Email: chenxiao-610@zju.edu.cn (X.C.); zwmao@zju.edu.cn (Z.M.); zhouyt@zju.edu.cn (Y.Z.)

The findings presented here provided new insights into the mechanism of tendon HO and established a powerful drug delivery system for treatment of tendon-related diseases. The targeted delivery of RAPA to pathological collagen could be a therapeutic approach for prevention of HO. It may also conceivably be used as an effective approach to prevent and treat other diseases associated with the destruction of collagen structure.

RESULTS

TSPCs participated in the formation of HO in the inflammatory niche

A mouse Achilles tendon HO model was induced by collagenase in this study. The inflammation followed the breakdown of the collagen matrix in the early stage and then receded because of the rodents' robust self-healing ability. Immunohistochemical staining indicated a marked increase in the expression of interleukin-1β (IL-1β) at 1 week after tendon injury, followed by a return to a near-normal level at 3 weeks (fig. S1A). However, the emergence of inflammation inevitably induced incorrect TSPC differentiation to eventually trigger HO formation. We then established Scx-cre;mTmG mice whose cells expressed red fluorescent protein (tdTomato) before exposure to Cre recombinase, while Cre-expressing cells and their derivatives would stop to express green fluorescent protein (GFP). Immunofluorescence (IF) following induction of the HO model with collagenase in these Scx-cre;mTmG mice revealed colocalization of GFP and the osteogenic differentiation–related gene bone morphogenic protein 2 (BMP2) (fig. S2A). GFP also colocalized with the chondrogenic differentiation–related gene SOX9 (fig. S2B). These findings indicated that TSPCs participated in the formation of HO under inflammatory conditions.

The mTOR signaling pathway was required for tendon HO

The role of mTOR in tendon HO was investigated further in a transgenic mouse model in which the mTOR gene was conditionally knocked out in the tendon lineage (for convenience, the Scx-Cre;mTOR^{floxed} mice are henceforth referred to as mTOR-TKO, for mTOR tendon knockout mice) (*16*). Collagenase was then injected into the Achilles tendon of mTOR^{floxed} [termed wild-type (WT) here for simplicity] mice or mTOR-TKO mice to obtain the HO model in both mouse types. After 6 weeks, significant high-intensity zones were observed on micro–computed tomography (micro-CT) images of Achilles tendon in the WT group (Fig. 1A). By contrast, the mTOR-TKO mice showed virtually none of these zones (Fig. 1B). Histological staining results, including hematoxylin and eosin (H&E), Masson trichrome (Masson), and Safranin O (SO) staining, also showed typical endochondral ossification in the WT mouse tendons, but not in the mTOR-TKO mouse tendons (Fig. 1, C to F). Isolation of TSPCs from WT and mTOR-TKO mice and culture in an osteogenic induction medium revealed reduced alkaline phosphatase (ALP) and Alizarin Red S (ARS) staining in the TSPCs from mTOR-TKO mice, indicating a weaker osteogenic differentiation ability than in the WT mice (Fig. 1, G to J). The TSPCs from mTOR-TKO mice also grew more poorly than WT TSPCs in the chondrogenic induction culture system (Fig. 1K). These findings confirmed that the osteogenesis and chondrogenesis ability of the injured tendon was sharply decreased at the tissue and cell level by knockout of mTOR signaling.

We then investigated potential molecular mechanisms involved in ossification via the mTOR signaling pathway by conducting RNA-sequencing (RNA-seq) studies on the tendon tissues. We used the WT mice as a reference and found 1261 down-regulated genes and 611 up-regulated genes in the mTOR-TKO group (fold change, ≥ 2; q value < 0.05) (Fig. 2A), which was consistent with the current knowledge about the function of the mTOR signaling pathway and its primary relationship with cell growth and anabolism (*10*). A subsequent comparison of the gene expression differences between the WT and mTOR-TKO mice (Fig. 2B and fig. S3A) and gene ontology (GO) analysis revealed that mTOR tendon knockout weakened cell osteogenesis and chondrogenesis, and it down-regulated genes related to tissue mineralization and ossification (Fig. 2C). Kyoto Encyclopedia of Genes and Genomes (KEGG) analysis showed that the top 20 down-regulated items in mTOR-TKO mice were those related to PI3K (phosphatidylinositol 3-kinase)–AKT, mitogen-activated protein kinase, insulin, and other signaling pathways (fig. S3B) reportedly involved in ectopic ossification development in tendons (*21*–*24*). A gene set enrichment analysis (GSEA) was also performed on all genes because of the inherent limitations of differentially expressed gene analysis. The results demonstrated that mTOR signaling was indeed down-regulated in the mTOR knockout mice and that the BMP signaling pathway and the response to BMP signals were both notable down-regulated (Fig. 2, D and E, and fig. S4A). BMP signaling is recognized as a crucial regulator of osteogenic differentiation of TSPCs (*25*, *26*). Overall, these in vivo and in vitro findings supported a role for mTOR signaling pathway in tendon HO.

RAPA attenuated osteogenesis and chondrogenesis of TSPCs in the inflammatory environment

An in vitro cell assay confirmed that 2 nM RAPA had a negligible effect on cell proliferation but effectively inhibited the expression of p-mTOR and p-S6 (Fig. 3, A and B). Stimulation of TSPCs in chondrogenic culture with IL-1β resulted in intensification of both Alcian blue and SO staining when compared with an unstimulated control group, suggesting an augmented expression of cell materials containing anionic groups, such as chondroitin sulfate and keratan sulfate (Fig. 3, C, D, G, and H). In other words, the ability of TSPCs to differentiate into chondrocytes was enhanced. The addition of RAPA blocked the effect induced by IL-1β (Fig. 3, C, D, G, and H). Similarly, when we used osteoinductive medium to induce osteogenesis of TSPCs, RAPA suppressed osteogenic differentiation of TSPCs induced by the IL-1β stimulation, as revealed by ALP and ARS staining (Fig. 3, E, F, I, and J). Human TSPCs showed similar RAPA responses (fig. S5, A to J). RAPA therefore prevented the abnormal differentiation of TSPCs under inflammatory stimulation by inhibiting the mTOR signaling pathway.

The mTOR had dual effects on TSPC differentiation

The mTOR pathway is critical for tendon development, as confirmed by the tendon defects observed due to tendon-specific ablation of mTOR in our mTOR-TKO mice and the impaired tenogenesis of mesenchymal stem cells by RAPA (*16*). The RNA-seq analysis results also indicated that the transforming growth factor–β (TGF-β) signaling pathway was down-regulated in mTOR-TKO mice (fig. S4B). Similar changes were also observed in tendon-related genes (fig. S4C). TGF-β controls a bidirectional regulatory pathway that participates in the process of tendon HO and in the promotion of tenogenesis in mesenchymal stem cells (*27*, *28*). We hypothesized that these dual actions of mTOR could also regulate the behavior of TSPCs. Treatment

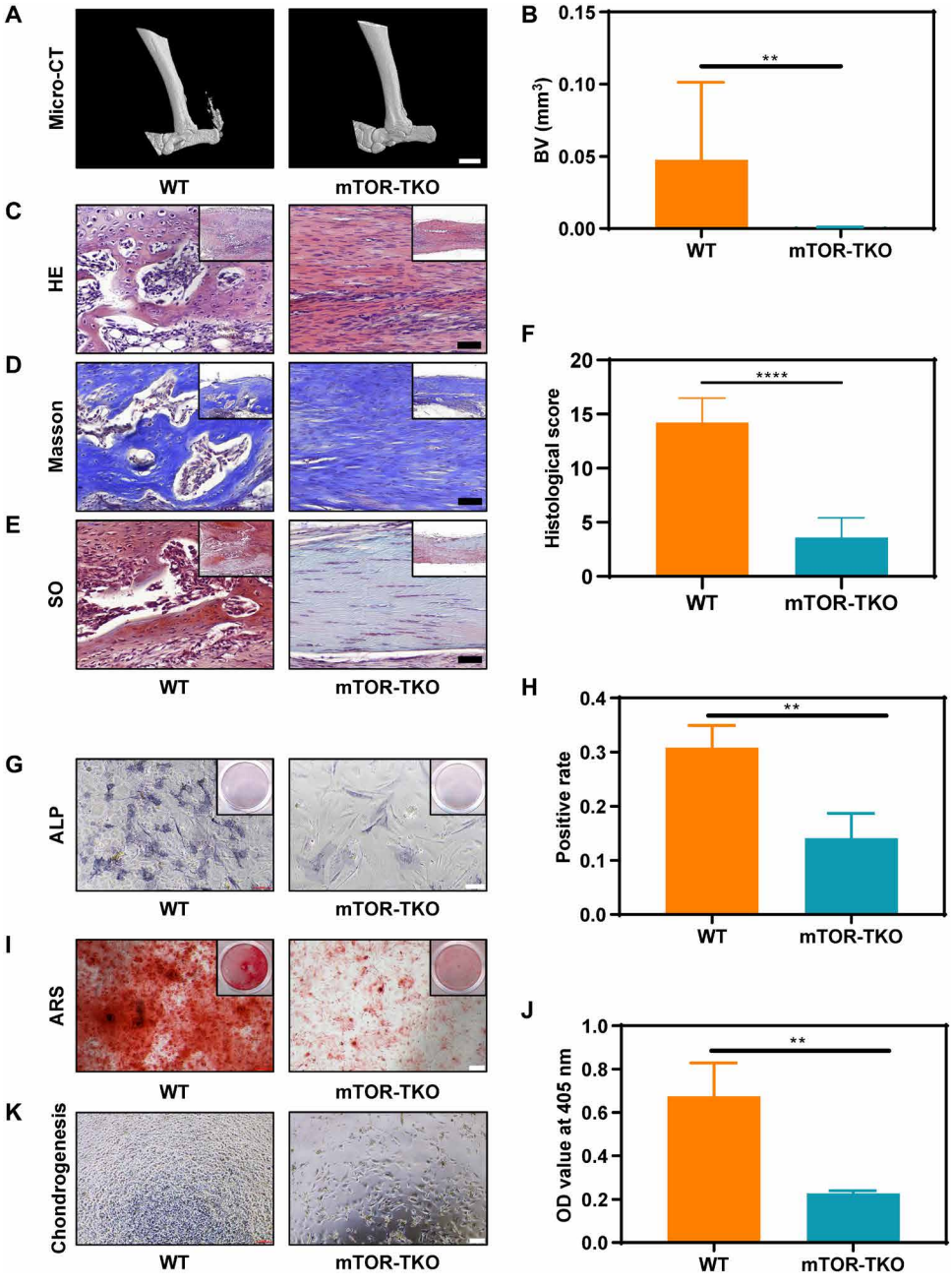

Fig. 1. The mTOR signaling pathway is required in tendon HO. (**A** and **B**) Micro-CT imaging and quantitative analysis of the Achilles tendon from WT and mTOR knockout (mTOR-TKO) mice. $n = 10$. Scale bar, 2 mm. (**C** to **F**) HE, Masson, and SO staining and histological score evaluation of WT and mTOR-TKO mice. $n = 10$. Scale bar, 50 μm. (**G** and **H**) ALP staining and positive rate of cells cultured in an osteogenic medium for 7 days. $n = 3$. Scale bars, 100 μm. (**I** and **J**) ARS staining and optical density (OD) value of cells cultured in the osteogenic medium for 14 days. $n = 3$. Scale bar, 200 μm. (**K**) Light microscopy of cells cultured in the chondrogenic medium for 3 days. BV, bone volume.

of TSPCs with high concentrations of RAPA inhibited TSPC proliferation, but the inhibitory effect disappeared upon withdrawal of RAPA (fig. S6A). RAPA at 2 nM also inhibited the expression of tendon-related genes in the TSPCs, and this expression was rapidly restored after drug withdrawal (fig. S6B). These findings indicated that the effects of RAPA were reversible.

CHP-PLGA-RAPA nanoparticles provided sustained release of RAPA to damaged tendon

CHP-PLGA nanoparticles were synthesized to provide targeted delivery and sustained release of RAPA at sites of tendon damage. The PLGA nanoparticles were prepared using an oil/water (O/W) emulsion-solvent evaporation method with bovine serum albumin

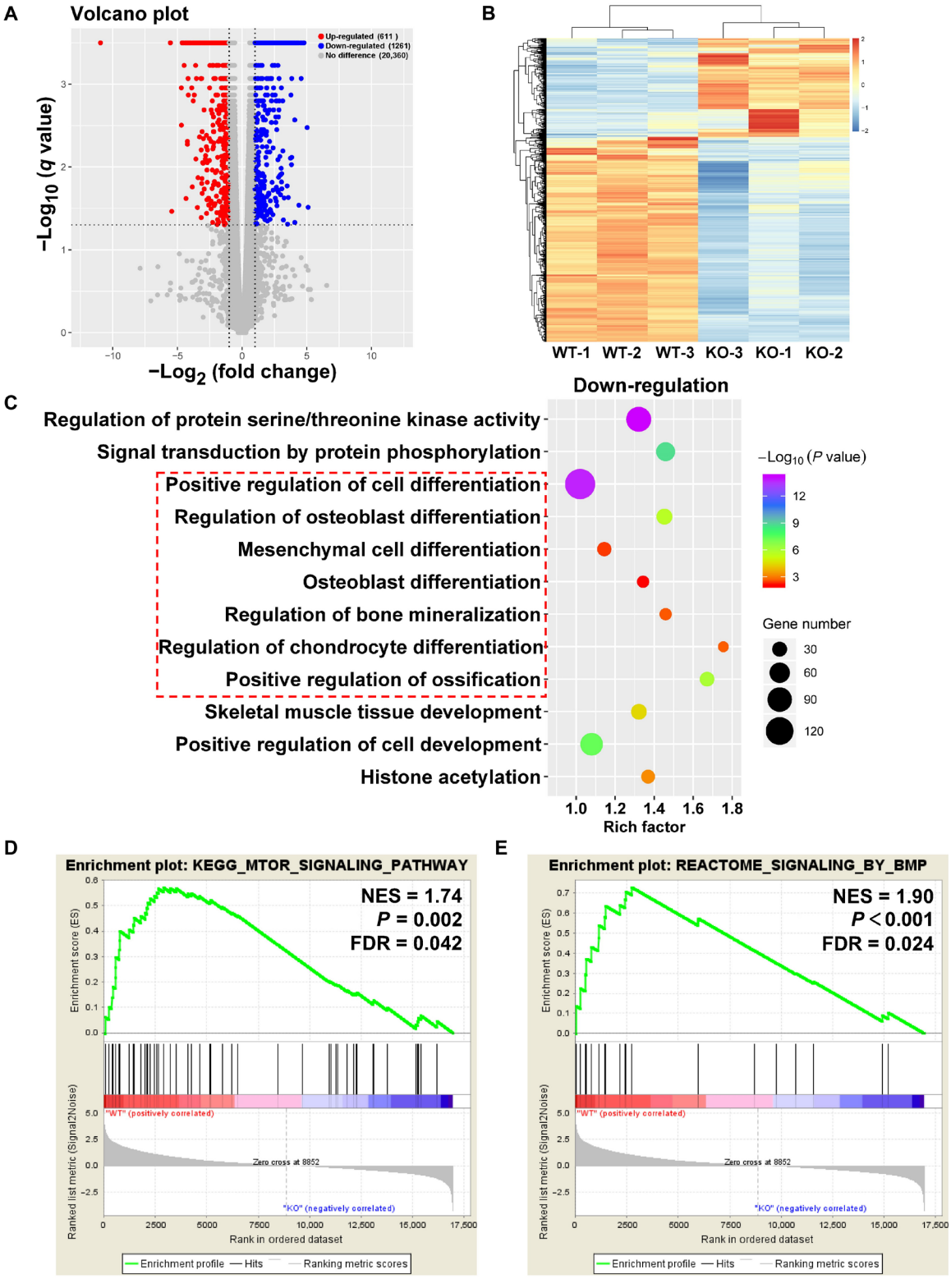

Fig. 2. RNA-seq analysis of tendon between WT and mTOR-knockout (mTOR-TKO) mice. (**A**) Volcano plot of gene expression (mTOR-TKO versus WT; fold change, ≥2; *q* value < 0.05). (**B**) Heat map of differentiated expression genes. (**C**) GO analysis of differentially expressed genes. (**D** and **E**) GSEA of the genes associated with mTOR signaling and BMP signaling. NES, normalized enrichment score; FDR, false discovery rate; KO, knockout.

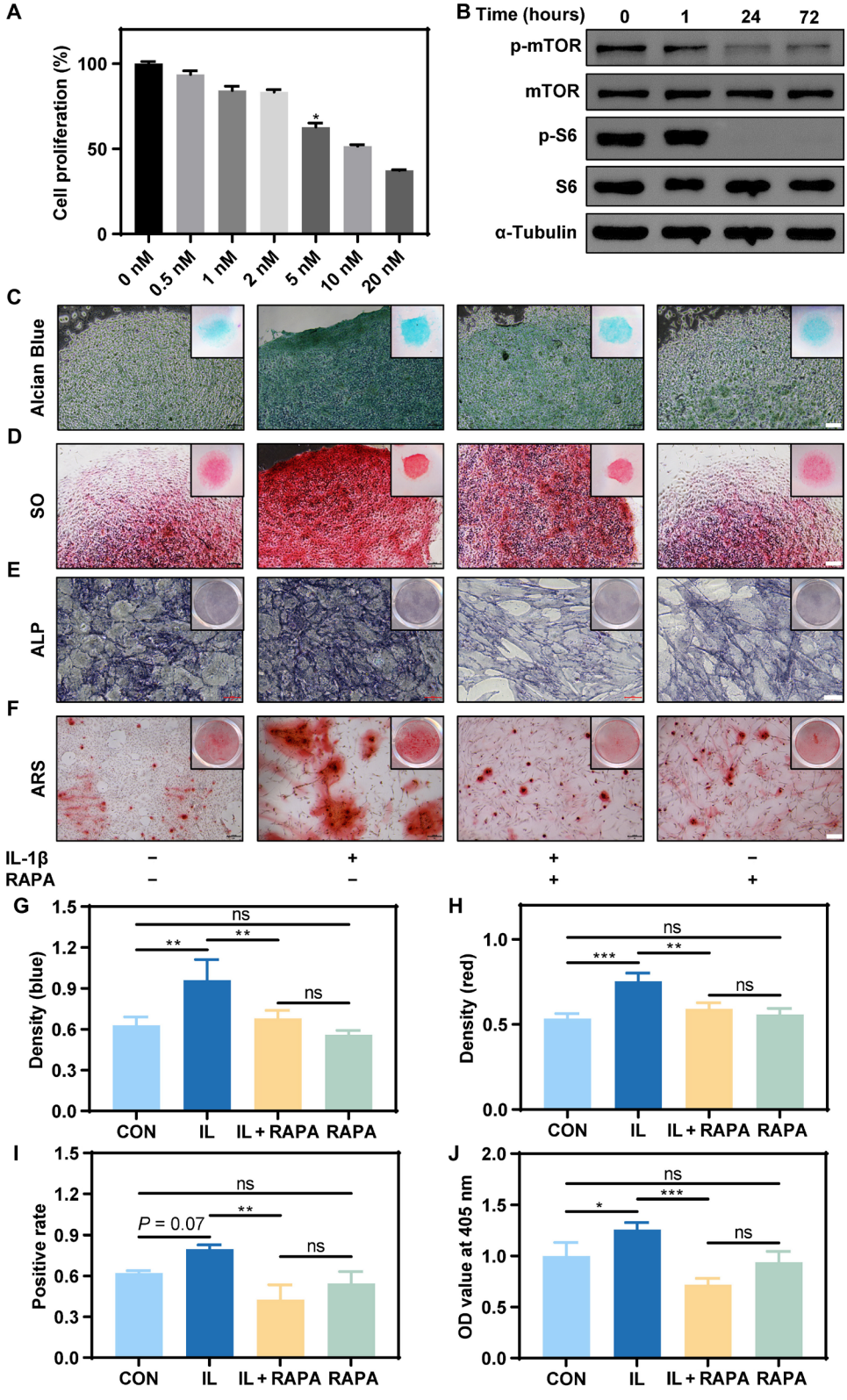

Fig. 3. RAPA inhibited osteogenesis and chondrogenesis of TSPCs induced by IL-1β. (**A**) Cell proliferation of TSPCs when cultured with different concentrations of RAPA. (**B**) The protein expression of mTOR signaling pathway, including p-mTOR, mTOR, p-S6, S6, and the reference protein α-tubulin. (**C** and **D**) Alcian blue and SO staining of TSPCs cultured in the chondrogenic medium for 14 days. Scale bars, 50 μm. (**E** and **F**) ALP and ARS staining of TSPCs cultured in the osteogenic medium for 7 and 14 days, respectively. Scale bars, 50 and 200 μm, respectively. (**G**) Optical density (blue) of Alcian blue staining. $n = 3$. ns, not significant. (**H**) Optical density (red) of SO staining. $n = 3$. (**I**) Positive rate of ALP staining. $n = 3$. (**J**) Optical density value of ARS staining. $n = 3$.

(BSA) molecules acting as stabilizers in the water phase. The BSA molecules covering the particle surface enabled the subsequent covalent conjugation of a peptide with amino groups using glutaraldehyde as a cross-linker. The obtained PLGA nanoparticles were spherically shaped, with diameters ranging from 100 to 300 nm in the dry state, as observed in scanning electron microscopy (SEM) and transmission electron microscopy (TEM) images (Fig. 4, A and B). The surface zeta potential of the PLGA nanoparticles was −18.9 mV (Fig. 4C) due to the surface cover with negatively charged BSA. The hydrophilic diameter of the PLGA nanoparticles was 227 ± 38 nm (Fig. 4D), which was larger than the dry-state diameter because of the hydration of the BSA surface coating.

As shown in Fig. 4 (E and F), the densities of immobilized CHP peptide molecules on the CHP-PLGA nanoparticles increased with increasing concentrations of the reagent in the feeding solution and with increasing reaction time. Specifically, the density of CHP reached 4.2×10^4 molecules per nanoparticle (i.e., approximately 0.6 molecule/nm^2) at a peptide feeding concentration of 80 μg/ml and a reaction time of 16 hours. These conditions produced a sufficiently high CHP density, so they were used in subsequent experiments.

The introduction of CHP onto the surface did not produce any obvious changes in the morphology, size, or surface zeta potential of the PLGA nanoparticles (Fig. 4, A to D). The loading ratios of RAPA for both PLGA and CHP-PLGA nanoparticles were quite similar (39 and 37 μg/mg, respectively) when subjected to the same incubation and washing processes. Approximately 14.7% of the loaded RAPA was released during the peptide conjugation process because this step takes a long time at room temperature. This release is actually advantageous since it enables a sustained release of RAPA because the initial burst release has already occurred. Both PLGA and CHP-PLGA showed a good sustained release of encapsulated RAPA, as determined by almost linear release curves versus time for more than 1 week (Fig. 4G). The RAPA was gradually released because of the degradation of the polymer matrix and its slow diffusion into the medium.

The ability of CHP-PLGA to target-bind to injured collagen was then evaluated in vitro by two methods (i.e., incubation of CHP-PLGA with collagen denatured by high temperature or with tendon damaged with collagenase). SEM and TEM observations revealed that the CHP coating aided the specific attachment of the CHP-PLGA nanoparticles to injured collagen or injured tendon, as attachment was rarely observed to intact collagen or intact tendon (Fig. 4, H and I). Incubation of PLGA and CHP-PLGA nanoparticles with normal and diseased human tendon also revealed binding of a large amount of CHP-PLGA to pathological collagen, but only a very small amount of nonspecific binding to healthy tendon, indicating a therapeutic potential of these nanoparticles in clinical practice (fig. S7A).

We then examined the biological activity of CHP-PLGA-RAPA nanoparticles. The culture medium was changed every other day, and the amount of RAPA released from the CHP-PLGA-RAPA nanoparticles was approximately 25% on the second day. Therefore, we increased the concentration of CHP-PLGA-RAPA to 8 nM to ensure that the total amount of RAPA released the next day was approximately equal to the amount previously used. The RAPA released from CHP-PLGA maintained its biological effect (i.e., it inhibited the mTOR signaling pathway, osteogenesis, and chondrogenesis of TSPCs following inflammatory stimulation; fig. S8, A to J). The CHP-PLGA-RAPA nanoparticles therefore showed potential as a drug delivery system for tendon disease with sustained-release ability, targeted binding, and biological function.

CHP-PLGA-RAPA effectively prevented tendon HO

The drug delivery efficiency of CHP-PLGA nanoparticles in pathological mouse tendon was evaluated by synthesizing CHP-PLGA-Cy5 nanoparticles and injecting them into mouse tendons after HO modeling. The replacement of RAPA with Cy5 allowed the detection of the nanoparticle cargo with infrared fluorescence imaging devices to provide general feedback regarding drug retention. The CHP-PLGA nanoparticles significantly enhanced the retention of Cy5 in the tendon tissue at various time points when compared with PLGA nanoparticles, indicating that the CHP coating provided a stronger affinity for damaged tendon and made the nanoparticles a more effective drug delivery vehicle (Fig. 5, A to C).

The HO model causes notable inflammation, so drug administration was halted at 3 weeks to allow the tendon tissue to pass through the inflammatory window without hindering the subsequent tendon repair process (Fig. 6A). The immunohistochemical results suggested a substantial down-regulation of the mTOR signaling pathway in the PLGA-RAPA and CHP-PLGA-RAPA treatment groups at 3 weeks (fig. S9A). At 6 weeks, micro-CT imaging indicated that PLGA-RAPA and especially CHP-PLGA-RAPA significantly decreased the occurrence of HO in the mouse tendons (Fig. 6, B and C). All histological evaluations, including HE, Masson, and SO staining, identified significant improvement in the sustained-release medication group. Moreover, little or no ectopic bone tissue was observed following CHP-PLGA-RAPA or PLGA-RAPA treatment (Fig. 6, D to G). The primary difference was that CHP-PLGA-RAPA almost completely inhibited endochondral ossification, whereas some chondroid tissues, which were not apparent in micro-CT images, appeared in the PLGA-RAPA group. Overall, the CHP-PLGA-RAPA nanoparticles showed good tissue-specific binding ability and were effective in preventing abnormal differentiation of TSPCs caused by an inflammatory microenvironment.

DISCUSSION

In this study, mTOR signaling was found to play a dominant role in tendon ectopic osteogenesis occurring both in vitro and in vivo. Because mTOR inhibition also influences the physiological tenogenesis of normal tendon, we established a mouse model of tendon HO, and we developed a drug delivery system that would target the diseased tendon tissue to reduce side effects on normal tendon. This drug delivery system almost completely inhibited the development of tendon HO in the mouse model.

Until now, our understanding of the mechanism underlying tendon HO has been limited. However, some studies have highlighted a possible involvement of mTOR in the process of tendon HO. For example, Hino *et al.* (*12*, *29*) reported that mTOR signaling upregulated aberrant chondrogenesis in fibrodysplasia ossificans progressiva disease. Similarly, Xu *et al.* (*13*) identified the AKT-mTOR pathway as a therapeutic target for the treatment of inflammation-mediated osteogenesis of stem cells in periodontal ligament. A rat HO model induced by Achilles tendon transection also indicated that RAPA modulated the osteogenesis of TSPCs (*14*). In the present study, the combination of an in vitro cell experiment with RNA-seq analysis and conditional gene knockout mice revealed that mTOR was an obligatory link in the tendon endochondral ossification

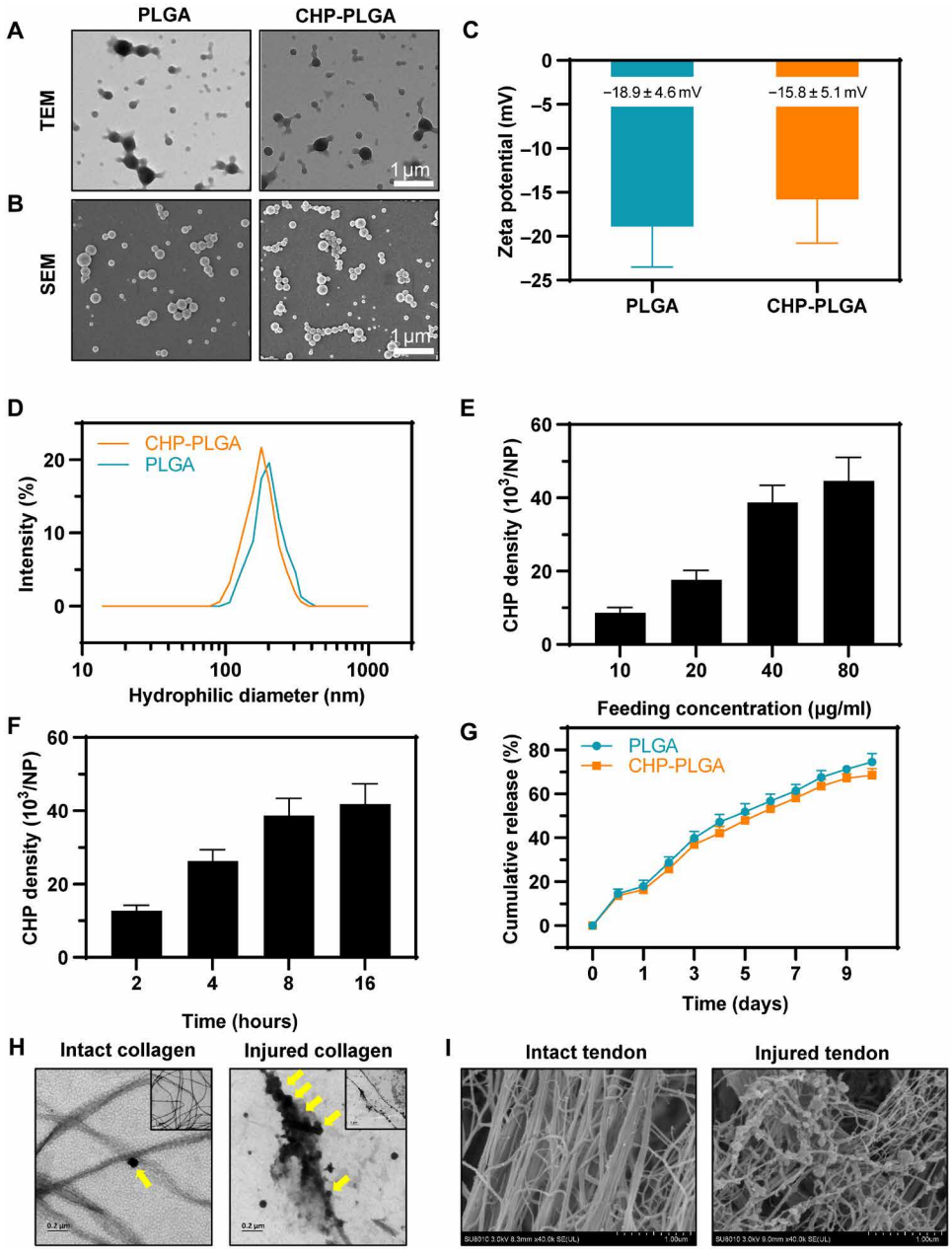

Fig. 4. Characterization of CHP-PLGA nanoparticles. (**A** and **B**) TEM and SEM images of PLGA and CHP-PGLA nanoparticles. Scale bars, 1 μm. (**C**) Zeta potential of PLGA and CHP-PLGA nanoparticles. $n = 4$. (**D**) Size distribution of PLGA and CHP-PLGA nanoparticles. (**E** and **F**) CHP density at various feeding concentrations and different times. $n = 4$. (**G**) Drug release from PLGA and CHP-PLGA nanoparticles over the course of 10 days. $n = 4$. (**H**) TEM of CHP-PLGA binding to intact and injured collagen. (**I**) SEM of CHP-PLGA binding to intact and injured tendon.

process. We observed that cells expressing the Scx gene were involved in ectopic osteogenesis, in agreement with previous research (*25*, *26*). The Scx gene serves as a marker for TSPCs, thereby confirming the participation of endogenous stem cells from the tendon in the development of tendon HO.

The levels of IL-1β notable increased in the disease model, indicating that inflammation initiated the abnormal differentiation of TSPCs. We also observed a temporary increase in the expression of IL-1β in tendon injury, which led to the final tendon ossification. These findings suggested that once stem cells are exposed to external stimuli, the activated differentiation process is irreversible. Hence, in patients with HO, more attention must be paid to preserving the stemness of endogenous stem cells while taking measures to block extrinsic causes of abnormal differentiation.

In this study, we exploited a tendinopathy characteristic, namely, that collagen would degrade following an injury, and we used CHP-PLGA as a drug carrier to deliver targeted slow-release RAPA to an injured tendon. To the best of our knowledge, this is the first documented use of CHP as a targeting tool with potential for treatment of tendon disease. When compared with traditional direct drug injection, this delivery system performs both sustained-release and diseased tissue target-binding functions. The sustained-release

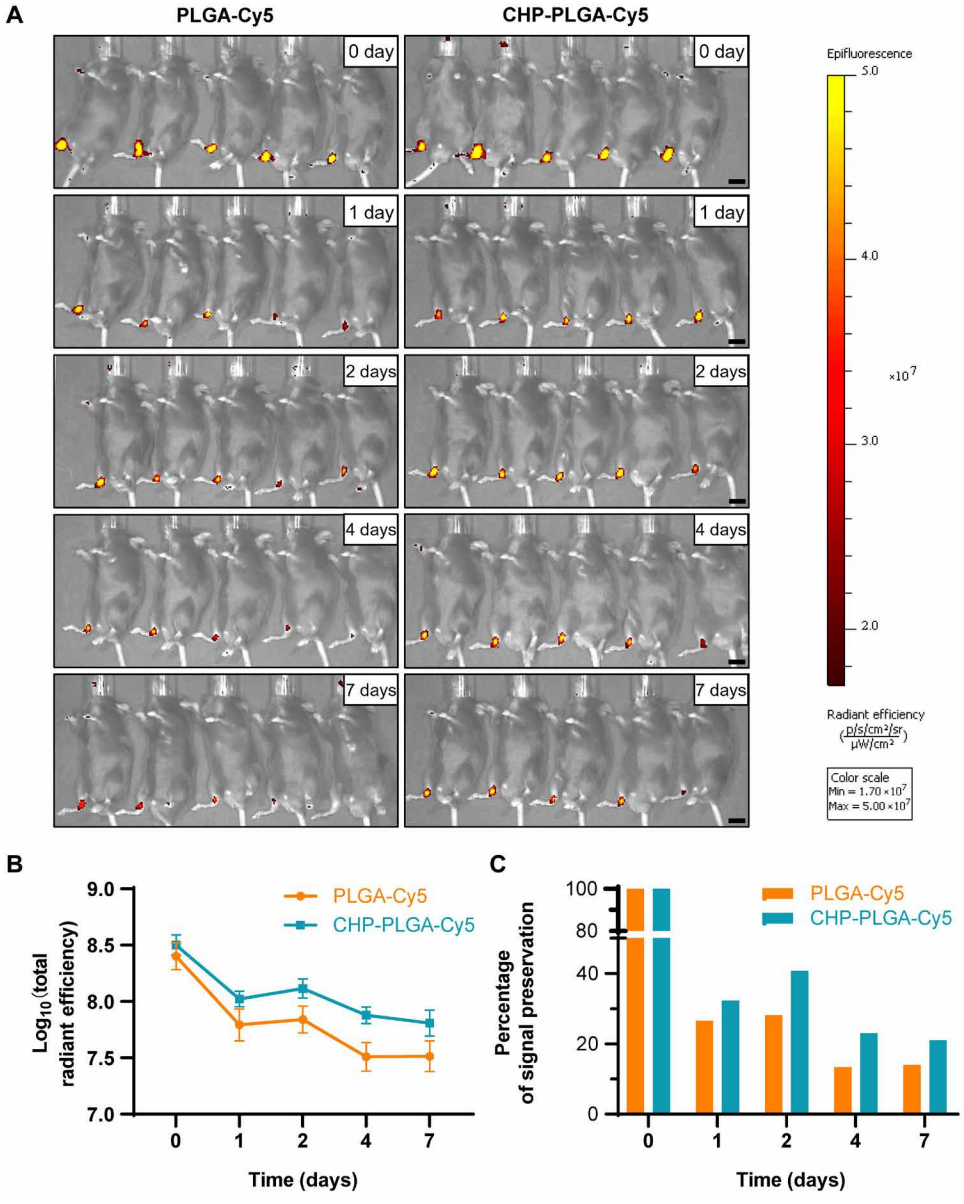

Fig. 5. In vivo assessment of pathological tendon-affinity ability of CHP-PLGA nanoparticles in a mouse model of tendon HO. (**A**) In vivo fluorescence images of injured Achilles tendon after subcutaneous injection of nanoparticles. Scale bars, 1 cm. (**B** and **C**) Total radiant efficiency and percentage of signal preservation of nanoparticles at different time points. $n = 5$.

property would greatly reduce the required frequency of drug injections in clinical practice. The specific binding of PLGA to pathological collagen imparted by the CHP coating means that patients could be given subcutaneous injections, thereby avoiding secondary injury due to tendon puncture. Microscopy observations indicated that CHP-PLGA may be more concentrated in and near the lesion, rather than randomly distributed throughout the tendon. If this also proves to be the case in a clinical situation, then this would substantially improve the sensitivity and effectiveness of the treatment and decrease possible side effects on normal tendons.

We speculated that the interaction of CHP with pathological tendon tissue was why CHP-PLGA exhibited greater potency than PLGA in the treatment of ectopic ossification of tendons, even though the PLGA-Cy5 study confirmed that PLGA nanoparticles were equally effective at retaining drugs. Moreover, unlike other antibodies that can only specifically target a certain type of collagen, CHP can target any type of denatured collagen chains and triple helix structures (*30*). In our study, HO was induced by collagenase, confirming that the collagen damage targeting mechanism works effectively.

Trauma in connective tissues is known to induce HO formation (*31*), and CHP would also be expected to target tendon damage due to trauma because injury would trigger an inflammatory reaction. Inflammatory factors, such as IL-1β and tumor necrosis factor–α, activate matrix metalloproteinases that degrade collagen, thereby

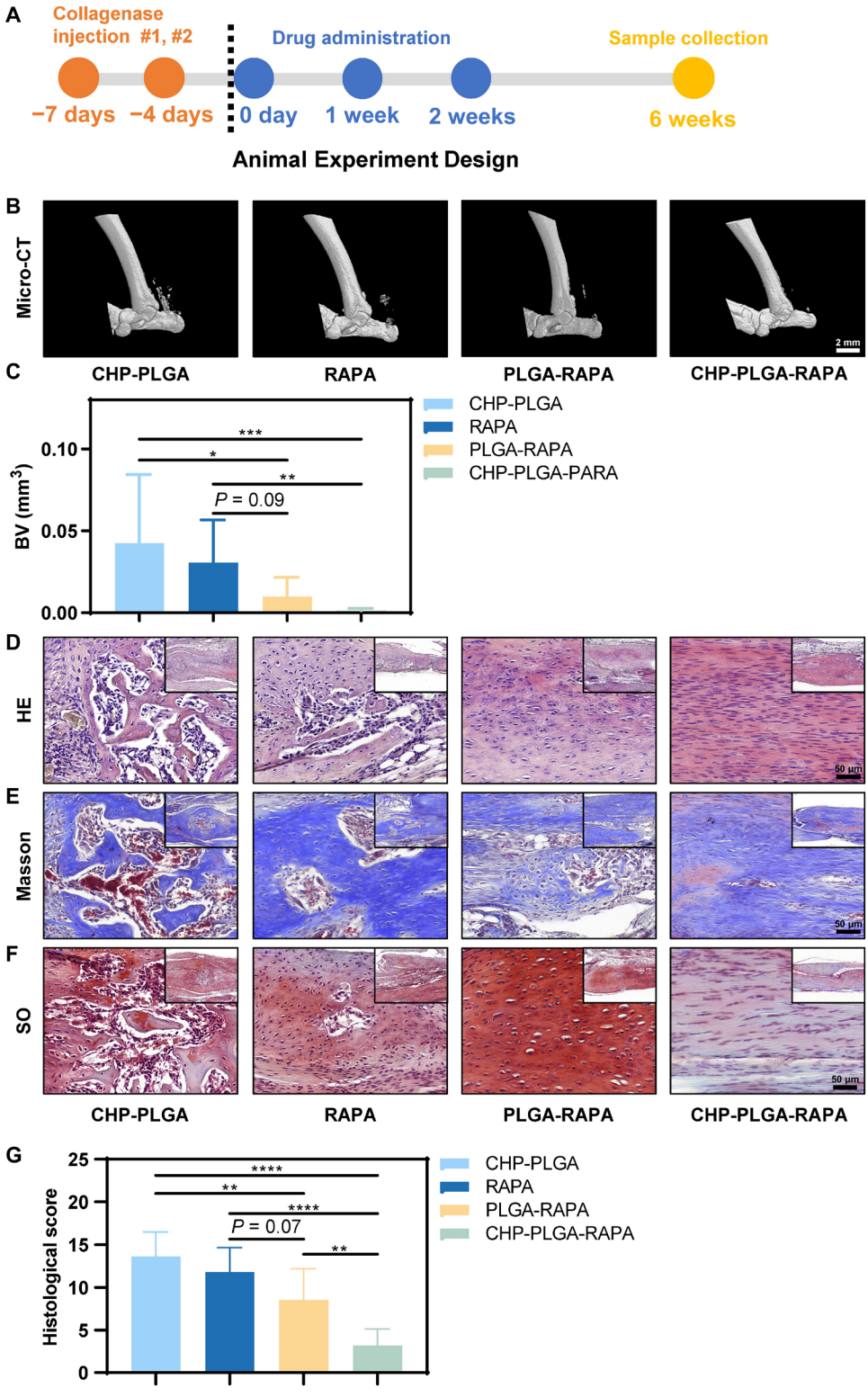

Fig. 6. In vivo assessment of pathological tendon protection ability of CHP-PLGA-RAPA nanoparticles in a mouse model of tendon HO. (**A**) Animal experiment design. (**B** and **C**) micro-CT images of the Achilles tendon at 6 weeks after HO modeling and quantitative analysis. *n* = 10. Scale bar, 2 mm. (**D** to **G**) HE, Masson, and SO staining and histological score evaluation of the Achilles tendon at 6 weeks. *n* = 10. Scale bars, 50 μm.

providing CHP with a target. Fibrodysplasia ossificans progressiva is a known HO disease of muscle and connective tissues (*29*), but HO in that disease is attributed to a mutation in the ACVR1 gene, with a pathological process unrelated to collagen fiber damage. In that type of collagen disease, the use of CHP may not be an effective strategy. Nevertheless, derivatives of CHP may also be available for the diagnosis and treatment of collagen degeneration–related diseases, such as osteoarthritis and intervertebral disc disease.

MATERIALS AND METHODS

Isolation and culture of TSPCs

The Achilles tendon in C57BL/6 mice and the remaining tendon graft tissues from autologous human tendon transplantation (i.e., from anterior cruciate ligament reconstruction surgery) were cut into pieces, digested with 0.2% type 1 collagenase, screened by low-density culture, and lastly cultured in a basic medium [low-glucose Dulbecco's modified Eagle's medium (L-DMEM), 10% fetal bovine serum (FBS), and 1% penicillin-streptomycin].

The osteogenic medium consisted of high-glucose DMEM (H-DMEM) containing 10^{-8} M dexamethasone, vitamin C (50 μg/ml), 10 mM β-glycerol phosphate, and 10% FBS. On day 7 of culture, the ALP activity of TSPCs was tested with a commercial detection kit (Beyotime, C3206). Cell nuclei were then stained with 4′,6-diamidino-2-phenylindole to count the total cell numbers and calculate the positive rates of ALP staining. On day 14, the calcium deposits formed by TSPCs were stained with ARS (Sigma-Aldrich, A5533). The stained nodules were solubilized with 5% SDS in 0.5 N HCl for 30 min at room temperature, and the optical density of the solution was determined at 405 nm.

The chondrogenic medium consisted of H-DMEM containing 1 mM sodium pyruvate, 1% Insulin-Transferrin-Selenium, vitamin C (50 μg/ml), 10^{-7} M dexamethasone, and TGF-β3 (10 ng/ml). Chondrogenesis was evaluated in a micromass culture system described previously (*32*). At day 14, cells were stained with Alcian blue or SO. The optical density (blue for Alcian blue and red for SO) of the microphotograph was analyzed using image analysis software (IPP 6.0).

The tenogenic medium was H-DMEM containing vitamin C (50 μg/ml) and 10% FBS. After the cells reached nearly 90% confluence, the basic medium was replaced with the induction medium, culture was continued for 14 days, and the TSPCs were then collected for RNA extraction and quantitative real-time polymerase chain reaction (qRT-PCR) analysis.

Cell proliferation assay

Cell proliferation was measured with a commercial kit (CCK-8, Dojindo, CK04). Briefly, TSCPs were incubated in a 10% CCK-8 solution at 37°C for 1 hour. The optical density of the solution was then measured at 450 nm with a microplate reader (SpectraMax 190, Molecular Devices).

Quantitative real-time polymerase chain reaction

TSPCs were lysed with TRIzol (Takara, 9109) to harvest total RNA, which was reverse-transcribed into complementary DNA (cDNA). The qRT-PCR was performed with a SYBR Green Mix (Takara, RR420A) in a fluorescence signal detection device (Roche, LightCycler 480).

The primers used in this analysis were the following:

Genes	5′-3′	Sequence
Mouse *Scx*	Forward	CCTTCTGCCTCAGCAACCAG
	Reverse	GGTCCAAAGTGGGGCTCTCCGTGACT
Mouse *Mkx*	Forward	CCCCGGACATCGGATCTACTA
	Reverse	CTCTTAGGATGAGGATTTAGGTA
Mouse *Tnmd*	Forward	GGGTGGTCCCGCAAGTGAAGGTG
	Reverse	GCCTCGACGACAGTAAATACAACAGT
Mouse *Dcn*	Forward	AGACTCACAGCCGAGTAGGA
	Reverse	ACATTCGCATCTCAGACACC
Mouse *Fmod*	Forward	CAATGTCTACACCGTCCCTGA
	Reverse	AGAAGGCTGCTGGAGTTGAAG
Mouse *Col1α1*	Forward	AACCCGAGGTATGCTTGATCT
	Reverse	CCAGTTCTTCATTGCATTGC
Mouse *Col3α1*	Forward	GCCTCCCAGAACATTACATAC
	Reverse	CAATGTCATAGGGTGCGATA
Mouse *Col14α1*	Forward	CGTGCTCTGCTTATGGCGTTG
	Reverse	ACGTGACAGCATTTGGTAAGTG
Mouse *Egr1*	Forward	CAGCGCCTTCAATCCTCAAG
	Reverse	GCGATGTCAGAAAAGGACTCTGT
Mouse *Fn1*	Forward	GCCACACCTACAACCAGTATACA
	Reverse	GGTGGGGCTGGAAAGATTACTC
Mouse *Gapdh*	Forward	ATACGGCTACAGCAACAGGG
	Reverse	TGTGAGGGAGATGCTCAGTG

Western blot analyses

The antibodies used in this study were the following: rabbit anti-mTOR [Cell Signaling Technology (CST), 2983], rabbit anti–p-mTOR (CST, 5536), rabbit anti-S6 (CST, 2217), and rabbit anti-pS6 (CST, 4858).

Preparation and characterization of nanoparticles

An ultrasonic liquid processor (MISONIX, USA) was used throughout the study to prepare PLGA (poly(lactic-co-glycolic acid) (lactic acid:glycolic acid = 75:25, M_w, ~78 kDa, Jinan Daigang Biomaterial Co. Ltd., China) nanoparticles using BSA (Sigma-Aldrich) as the emulsifier. Briefly, PLGA and RAPA (S1039, Selleck) were dissolved in dichloromethane at 20 and 1 mg/ml, respectively. A 1-ml volume of the PLGA/RAPA mixture was quickly added to 4 ml of emulsifier solution (3% BSA, aqueous solution) under vigorous magnetic stirring, followed by probe sonication at 10 W for 30 s on ice to complete the emulsification. This O/W emulsion was then dispersed into a 20-fold volume of Milli-Q water and stirred for at least 3 hours until it solidified. The resulting BSA/PLGA nanoparticles were then collected, purified by centrifugation at 12,000 rpm for 10 min, and resuspended in Milli-Q water three times to remove residual non-incorporated BSA molecules.

CHP was covalently conjugated to the BSA-coated PLGA nanoparticles using glutaraldehyde chemistry. Before preparation, the helix structure of the CHP peptide was disassembled by heating to 80°C for 5 min and then cooling on ice for 1 min. The suspension of PLGA nanoparticles (1 mg/ml) was mixed with glutaraldehyde (final concentration of 1 mg/ml) for 12 hours at room temperature under gentle shaking. During this step, one aldehyde group from the glutaraldehyde molecule reacted with amino groups from the BSA on the surface of PLGA nanoparticles. Since the amount of glutaraldehyde was in excess of that of BSA [PLGA nanoparticles

(about 50 μg/mg)], the cross-linking of BSA molecules was avoided. After centrifugation and washing again with water, the CHP peptide was added to the system. Further conjugation was allowed to occur between amino groups from peptide and the aldehyde groups on the PLGA nanoparticles for a certain period of time at room temperature. The peptide-modified PLGA nanoparticles were collected by centrifugation at 12,000 rpm for 10 min and washed with water three times to remove unbound CHP peptide molecules.

The fluorescence intensity of a fluorescein isothiocyanate (FITC)–labeled peptide solution before and after this reaction was compared to allow fluorescence spectroscopy assessment (LS55, PerkinElmer, USA) of the amount of bound peptide. In a typical experiment, PLGA nanoparticles (1 mg/ml) were activated with glutaraldehyde and then mixed with FITC-labeled peptide for conjugation. The initial solution volume and fluorescence intensity of the solution were recorded and denoted as V_i and F_i, respectively. After reaction and washing, all the medium was collected. This second volume and corresponding fluorescence intensity were designated as V_a and F_a, respectively. The amount of conjugated peptide was calculated according to the equation: $\Delta m = V_iF_i - V_aF_a$, and was determined by reference to a standard curve derived from fluorescence intensity versus peptide concentration.

The concentration of the different PLGA nanoparticles was determined by weighing the dried particles obtained from 1 ml of the suspension solution. The PLGA nanoparticle solution (100 μg/ml) was then used to measure the hydrodynamic diameters and the surface zeta potential in Milli-Q water (Beckman Delsa Nano, Beckman Coulter). The morphology of PLGA nanoparticles was observed by SEM and TEM.

The release of RAPA from the PLGA nanoparticles was monitored in phosphate-buffered saline (PBS; pH 7.4) at 37°C under gentle shaking. In brief, 1 ml of PLGA nanoparticles (1 mg/ml) was transferred to a dialysis bag (10-kDa cutoff; Sigma-Aldrich) and immersed into 10 ml of release buffer. At predetermined time intervals, 0.5 ml of release buffer was removed for measurement, and the same amount of fresh buffer was added back. The concentration of released RAPA was determined with a high-performance liquid chromatography system equipped with a Diamonsil C18 column (150 mm by 4.6 mm, 5 μm; Dikma Technologies Inc., Lake Forest, CA, USA) and a Hitachi L-2130 pump and L-2400 ultraviolet (UV) detector (Hitachi, Tokyo, Japan). The mobile phase was methanol and water (75:25, v/v) delivered at a flow rate of 1.0 ml/min. The UV detection wavelength was 278 nm, the column temperature was 50°C, and the injection volume was 20 μl.

Binding specificity of CHP-PLGA

Type 1 collagen (0.5 mg/ml in PBS) was denatured by heating at 80°C for 5 min and then placed in an ice bath. Mouse tendons were damaged by digestion with 2% collagenase for 30 min in a 37°C incubator. A 10-μl sample of injured type 1 collagen or 10 μl of intact type 1 collagen was added to a TEM grid. After 1 min, the excess solution was removed with blotting paper, and 10 μl of PLGA or CHP-PLGA nanoparticles (10 nM) was applied. The grid was incubated for 10 min and then washed three times with double-distilled water. The final sample was stained with 2% (w/v) uranyl acetate by applying 10 μl of staining solution to the grid and removing the excess solution with blotting paper after 1 min. The grid was dried at room temperature overnight and then observed by TEM. Intact tendons and injured tendons were subsequently incubated with CHP-PLGA (10 μM) for 2 hours on a shaking table at room temperature. The tendons were washed with PBS three times and further processed for SEM.

Animal experiments

Animal experiments were conducted with the approval of the Zhejiang University Experimental Animal Welfare and Ethics Committee under Institutional Animal Care and Use Committee guidelines (ZJU20190049). The tendon HO model was established by injecting type 1 collagenase (12.5 U per leg; Gibco, 17100017) into the midpoint of the right Achilles tendons of 8-week-old mice, and the same operation was repeated 3 days later to stabilize the effect. Ten WT mice and 10 mTOR-TKO mice were euthanized at 6 weeks after modeling, and the legs were removed for micro-CT imaging and subsequent histology.

In an in vivo drug experiment, 60 mice were divided equally into four groups, and each mouse received a subcutaneous injection (between Achilles tendon and skin) once per week: control group (sterile PBS, 5 μl), RAPA group (RAPA, 70 μM, 5 μl), PLGA-RAPA group (70 μM, 5 μl), and CHP-PLGA-RAPA group (70 μM, 5 μl). At 3 weeks after treatment, five mice in each group were euthanized for immunohistochemistry (IHC). At 6 weeks after treatment, the remaining 10 mice in each group were euthanized, and the legs were taken for micro-CT imaging and subsequent histology.

In an in vivo cell tracing experiment, three WT mice and three Scx-cre;mTmG mice were euthanized at 6 weeks after modeling. Achilles tendons were then isolated and prepared in paraffin sections for IF studies.

micro-CT imaging and analysis

Hindlimbs from the mice were fixed in 4% paraformaldehyde and analyzed by micro-CT (Skyscan 1172). The scanner was set at a voltage of 80 kV and a resolution of 18 μm per pixel. The images were reconstructed, analyzed for HO bone volume, and visualized by NRecon, CTAn, and CTVol.

In vivo fluorescence imaging and analysis

RAPA was replaced with Cy5 (Lumiprobe, 23020) in the synthesis process of PLGA-RAPA or CHP-PLGA-RAPA to obtain PLGA-Cy5 or CHP-PLGA-Cy5 nanoparticles, respectively. At 1 week after HO modeling, mice were injected with PLGA-Cy5 or CHP-PLGA-Cy5 and then anesthetized with isoflurane. The in vivo nanoparticle distribution was analyzed with a fluorescence imaging system (IVIS SpectrumCT, PerkinElmer) at the indicated time points.

Histology, IHC, and IF assays

Tissue specimens were fixed in 4% paraformaldehyde, washed with running water, dehydrated in a graded ethanol series, vitrified with dimethylbenzene, and embedded in paraffin. Paraffin sections (7 μm) were deparaffinized in xylene, hydrated with gradient ethanol, and stained with standard H&E, SO, or Masson staining procedures. Histological scores were calculated from the results of H&E staining.

For IHC or IF analysis, sections were incubated at 4°C overnight with primary antibodies. The following primary antibodies were used in this study: rabbit anti-GFP (CST, 2555), mouse anti-GFP (CST, AG281), rabbit anti-BMP2 (Beyotime, AF0075), mouse anti-SOX9 (Abcam, ab76997), rabbit anti-mTOR (CST, 2983), rabbit anti–p-mTOR (CST, 5536), rabbit anti-S6 (CST, 2217), rabbit anti-pS6 (CST, 4858), and rabbit anti–IL-1β (Abcam, ab9722). For IHC, the

sections were also incubated with horseradish peroxidase–linked secondary antibodies (CST, 7074) for 1.5 hours, and the staining was visualized with 3,3′-diaminobenzidine solution (ZSGB-BIO, ZLI-9017). For IF, sections were subsequently incubated with fluorescein-conjugated secondary antibodies for 1.5 hours and observed under a confocal fluorescence microscope (Nikon A1R, Japan).

RNA sequencing

Tendon tissues from WT and mTOR-TKO mice were ground in TRIzol to prevent RNA degradation. After verification of the RNA integrity, the extracted RNA was reverse-transcribed to create a cDNA library for subsequent sequencing.

Statistical analysis

The quantitative data were presented as means ± SD. Student's *t* test was performed to assess whether statistical differences existed between groups. Multiple comparisons were performed with a one-way analysis of variance (ANOVA) and Tukey's post-test. P values <0.05 were considered statistically significant. The significance level is presented as $^{*}P < 0.05$, $^{**}P < 0.01$, $^{***}P < 0.001$, and $^{****}P < 0.0001$.

SUPPLEMENTARY MATERIALS

Supplementary material for this article is available at http://advances.sciencemag.org/cgi/content/full/6/18/eaay9526/DC1

REFERENCES AND NOTES

1. N. L. Millar, G. A. Murrell, I. B. McInnes, Inflammatory mechanisms in tendinopathy - towards translation. *Nat. Rev. Rheumatol.* **13**, 110–122 (2017).
2. N. Maffulli, A. G. Via, F. Oliva, Chronic Achilles tendon disorders: Tendinopathy and chronic rupture. *Clin. Sports Med.* **34**, 607–624 (2015).
3. J. F. Kaux, B. Forthomme, C. L. Goff, J. M. Crielaard, J. L. Croisier, Current opinions on tendinopathy. *J. Sports Sci. Med.* **10**, 238–253 (2011).
4. G. Nourissat, F. Berenbaum, D. Duprez, Tendon injury: from biology to tendon repair. *Nat. Rev. Rheumatol.* **11**, 223–233 (2015).
5. D. Magne, C. Bougault, What understanding tendon cell differentiation can teach us about pathological tendon ossification. *Histol. Histopathol.* **30**, 901–910 (2015).
6. H. K. Uhthoff, K. Sarkar, J. A. Maynard, Calcifying tendinitis: a new concept of its pathogenesis. *Clin. Orthop. Relat. Res.* **1976**, 164–168 (1976).
7. S. Fenwick, R. Harrall, R. Hackney, S. Bord, A. Horner, B. Hazelman, G. Riley, Endochondral ossification in Achilles and patella tendinopathy. *Rheumatology* **41**, 474–476 (2002).
8. M. de Mos, W. Koevoet, H. T. van Schie, N. Kops, H. Jahr, J. A. Verhaar, G. J. van Osch, In vitro model to study chondrogenic differentiation in tendinopathy. *Am. J. Sports Med.* **37**, 1214–1222 (2009).
9. J. J. Hu, Z. Yin, W. L. Shen, Y. B. Xie, T. Zhu, P. Lu, Y. Z. Cai, M. J. Kong, B. C. Heng, Y. T. Zhou, W. S. Chen, X. Chen, H. W. Quyang, Pharmacological regulation of in situ tissue stem cells differentiation for soft tissue calcification treatment. *Stem Cells* **34**, 1083–1096 (2016).
10. R. A. Saxton, D. M. Sabatini, mTOR signaling in growth, metabolism, and disease. *Cell* **169**, 361–371 (2017).
11. Y. Zhao, M. M. Zhao, Y. Cai, M. F. Zheng, W. L. Sun, S. Y. Zhang, W. Kong, J. Gu, X. Wang, M. J. Xu, Mammalian target of rapamycin signaling inhibition ameliorates vascular calcification via Klotho upregulation. *Kidney Int.* **88**, 711–721 (2015).
12. K. Hino, K. Horigome, M. Nishio, S. Komura, S. Nagata, C. Zhao, Y. Jin, K. Kawakami, Y. Yamada, A. Ohta, J. Toguchida, M. Ikeya, Activin-A enhances mTOR signaling to promote aberrant chondrogenesis in fibrodysplasia ossificans progressiva. *J. Clin. Invest.* **127**, 3339–3352 (2017).
13. X.-Y. Xu, X.-T. He, J. Wang, X. Li, Y. Xia, Y.-Z. Tan, F.-M. Chen, Role of the P2X7 receptor in inflammation-mediated changes in the osteogenesis of periodontal ligament stem cells. *Cell Death Dis.* **10**, 20 (2019).
14. H. Jiang, Y. Chen, G. Chen, X. Tian, J. Tang, L. Luo, M. Huang, B. Yan, X. Ao, W. Zhou, L. Wang, X. Bai, Z. Zhang, L. Wang, C. J. Xian, Leptin accelerates the pathogenesis of heterotopic ossification in rat tendon tissues via mTORC1 signaling. *J. Cell. Physiol.* **233**, 1017–1028 (2018).
15. Y. Han, Y. Hong, L. Li, T. Li, Z. Zhang, J. Wang, H. Xia, Y. Tang, Z. Shi, X. Han, T. Chen, Q. Liu, M. Zhang, K. Zhang, W. Hong, Y. Xue, A transcriptome-level study identifies changing expression profiles for ossification of the ligamentum flavum of the spine. *Mol. Ther. Nucleic Acids* **12**, 872–883 (2018).
16. X. X. Cong, X. S. Rao, J. X. Lin, X. C. Liu, G. A. Zhang, X. K. Gao, M. Y. He, W. L. Shen, W. Fan, D. Pioletti, L. L. Zheng, J. H. Liu, Z. Yin, B. C. Low, R. Schweitzer, H. Ouyang, X. Chen, Y. T. Zhou, Activation of AKT-mTOR signaling directs tenogenesis of mesenchymal stem cells. *Stem Cells* **36**, 527–539 (2018).
17. M. Tsuzaki, G. Guyton, W. Garrett, J. M. Archambault, W. Herzog, L. Almekinders, D. Bynum, X. Yang, A. J. Banes, IL-1β induces COX2, MMP-1, –3 and –13, ADAMTS-4, IL-1β and IL-6 in human tendon cells. *J. Orthop. Res.* **21**, 256–264 (2003).
18. Y. Li, C. A. Foss, D. D. Summerfield, J. J. Doyle, C. M. Torok, H. C. Dietz, M. G. Pomper, S. M. Yu, Targeting collagen strands by photo-triggered triple-helix hybridization. *Proc. Natl. Acad. Sci. U.S.A.* **109**, 14767–14772 (2012).
19. J. Hwang, Y. Huang, T. J. Burwell, N. C. Peterson, J. Connor, S. J. Weiss, S. M. Yu, Y. Li, In situ imaging of tissue remodeling with collagen hybridizing peptides. *ACS Nano* **11**, 9825–9835 (2017).
20. B. H. San, Y. Li, E. B. Tarbet, S. M. Yu, Nanoparticle assembly and gelatin binding mediated by triple helical collagen mimetic peptide. *ACS Appl. Mater. Interfaces* **8**, 19907–19915 (2016).
21. T. Wang, C. Thien, C. Wang, M. Ni, J. Gao, A. Wang, Q. Jiang, R. S. Tuan, Q. Zheng, M. H. Zheng, 3D uniaxial mechanical stimulation induces tenogenic differentiation of tendon-derived stem cells through a PI3K/AKT signaling pathway. *FASEB J.* **32**, 4804–4814 (2018).
22. W. Zhou, X. Lin, J. Chu, T. Jiang, H. Zhao, B. Yan, Z. Zhang, Magnolol prevents ossified tendinopathy by inhibiting PGE2-induced osteogenic differentiation of TDSCs. *Int. Immunopharmacol.* **70**, 117–124 (2019).
23. K. Ranganathan, J. Peterson, S. Agarwal, E. Oluwatobi, S. Loder, J. A. Forsberg, T. A. Davis, S. R. Buchman, S. C. Wang, B. Levi, Role of gender in burn-induced heterotopic ossification and mesenchymal cell osteogenic differentiation. *Plast. Reconstr. Surg.* **135**, 1631–1641 (2015).
24. P. Han, Q. Cui, W. Lu, S. Yang, M. Shi, Z. Li, P. Gao, B. Xu, Z. Li, Hepatocyte growth factor plays a dual role in tendon-derived stem cell proliferation, migration, and differentiation. *J. Cell. Physiol.* **234**, 17382–17391 (2019).
25. D. Dey, J. Bagarova, S. J. Hatsell, K. A. Armstrong, L. Huang, J. Ermann, A. J. Vonner, Y. Shen, A. H. Mohedas, A. Lee, E. M. Eekhoff, A. van Shie, M. B. Demay, C. Keller, A. J. Wagers, A. N. Economides, P. B. Yu, Two tissue-resident progenitor lineages drive distinct phenotypes of heterotopic ossification. *Sci. Transl. Med.* **8**, 366ra163 (2016).
26. S. Agarwal, S. J. Loder, D. Cholok, J. Peterson, J. Li, C. Breuler, R. Cameron Brownley, H. Hsin Sung, M. T. Chung, N. Kamiya, S. Li, B. Zhao, V. Kaartinen, T. A. Davis, A. T. Qureshi, E. Shipani, Y. Mishina, B. Levi, Scleraxis-lineage cells contribute to ectopic bone formation in muscle and tendon. *Stem Cells* **35**, 705–710 (2017).
27. X. Wang, F. Li, L. Xie, J. Crane, G. Zhen, Y. Mishina, R. Deng, B. Gao, H. Chen, S. Liu, P. Yang, M. Gao, M. Tu, Y. Wang, M. Wan, C. Fan, X. Cao, Inhibition of overactive TGF-β attenuates progression of heterotopic ossification in mice. *Nat. Commun.* **9**, 551 (2018).
28. H. Liu, C. Zhang, S. Zhu, P. Lu, T. Zhu, X. Gong, Z. Zhang, J. Hu, Z. Yin, B. C. Heng, X. Chen, H. W. Ouyang, Mohawk promotes the tenogenesis of mesenchymal stem cells through activation of the TGFβ signaling pathway. *Stem Cells* **33**, 443–455 (2015).
29. K. Hino, C. Zhao, K. Horigome, M. Nishio, Y. Okanishi, S. Nagata, S. Komura, Y. Yamada, J. Toguchida, A. Ohta, M. Ikeya, An mTOR signaling modulator suppressed heterotopic ossification of fibrodysplasia ossificans progressiva. *Stem Cell Rep.* **11**, 1106–1119 (2018).
30. J. L. Zitnay, Y. Li, Z. Qin, B. H. San, B. Depalle, S. P. Reese, M. J. Buehler, S. M. Yu, J. A. Weiss, Molecular level detection and localization of mechanical damage in collagen enabled by collagen hybridizing peptides. *Nat. Commun.* **8**, 14913 (2017).
31. A. T. Qureshi, D. Dey, E. M. Sanders, J. G. Seavey, A. M. Tomasino, K. Moss, B. Wheatley, D. Cholok, S. Loder, J. Li, B. Levi, T. A. Davis, Inhibition of mammalian target of rapamycin signaling with rapamycin prevents trauma-induced heterotopic ossification. *Am. J. Pathol.* **187**, 2536–2545 (2017).
32. Y. Wang, X. Zhang, H. Huang, Y. Xia, Y. Yao, A. F. Mak, P. S. Yung, K. M. Chan, L. Wang, C. Zhang, Y. Huang, K. K. Mak, Osteocalcin expressing cells from tendon sheaths in mice contribute to tendon repair by activating Hedgehog signaling. *eLife* **6**, e30474 (2017).

Acknowledgments

Funding: This work was supported by the National Key Research and Development program of China (2018YFC1105100 and 2016YFE0132700), the NSFC grants (81972099, 81522029, 81772418, 31570987, 81871764, 81572157, 51822306, 31571402, 81572115, and 81874019), the Zhejiang Provincial Natural Science Foundation of China (LR20H060002), and the Fundamental Research Funds for the Central Universities (2019QNA7040). We are grateful to the Core Facilities of Zhejiang University School of Medicine, and Bio-Ultrastructure Analysis

Lab. of Analysis Center of Agrobiology and Environmental Sciences of the Zhejiang University for technical assistance. **Author contributions:** Conception: Y.C., W.S., Y.Z., Z.M., and X.C. Research design: Y.C., W.S., and X.C. Data acquisition/analysis: Y.C., W.S., C.T., J.H., C.F., Z.Y., Y.H., and Z.M. Resource assistance: W.C., H.O., Y.Z., Z.M., and X.C. Writing, drafting, and editing: Y.C., W.S., Y.Z., Z.M., and X.C. **Competing interests:** The authors declare that they have no competing interests. **Data and materials availability:** All data needed to evaluate the conclusions in the paper are present in the paper and/or the Supplementary Materials. Additional data related to this paper may be requested from the authors.

Submitted 31 July 2019
Accepted 7 February 2020
Published 29 April 2020
10.1126/sciadv.aay9526

Citation: Y. Chen, W. Shen, C. Tang, J. Huang, C. Fan, Z. Yin, Y. Hu, W. Chen, H. Ouyang, Y. Zhou, Z. Mao, X. Chen, Targeted pathological collagen delivery of sustained-release rapamycin to prevent heterotopic ossification. *Sci. Adv*. **6**, eaay9526 (2020).